Large-scale shell model study of β^{-}-decay properties of N = 126, 125 nuclei along the r-process path

Anil Kumar

Center for Computational Sciences
University of Tsukuba, Japan

筑波大学
計算科学研究センター
Center for Computational Sciences

Collaborators:

N. Shimizu (CCS, Tsukuba Univ.), Y. Utsuno (JAEA), P. C. Srivastava (IITR), and C. Yuan (SYSU)

Rising Research Seminar Series, November 12, 2024

Outline

Nucleosynthesis of heavy elements: competition b/w neutron capture and β decay

The origin of most atomic nuclei with masses heavier than the iron group elements is attributed to **neutron capture** nucleosynthesis

slow neutron capture process (s-process)

neutron capture << beta decay.
– Isotopes near stability are synthesized.

rapid neutron capture process (r-process)

neutron capture >> beta decay.
– Explosive environment!
– High temperatures ($T \approx 10^9$ K), and neutron densities ($> 10^{20}$ neutrons/cm^3).
– Isotopes far from stability are synthesized.

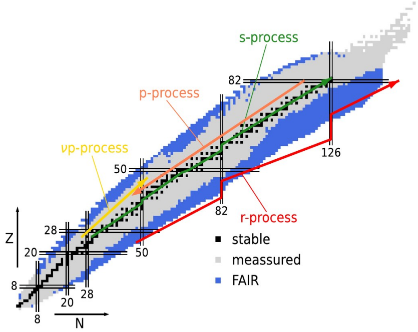

Fig. taken: A. Arcones et al., Astron Astrophys Rev **31**, 1 (2023).

T. Kajino et al., Progress in Particle and Nuclear Physics **107**, 109 (2019).

Nucleosynthesis of heavy elements: competition b/w neutron capture and β decay

The origin of most atomic nuclei with masses heavier than the iron group elements is attributed to **neutron capture** nucleosynthesis

slow neutron capture process (s-process)

neutron capture << beta decay.
– Isotopes near stability are synthesized.

rapid neutron capture process (r-process)

neutron capture >> beta decay.
– Explosive environment!
– High temperatures ($T \approx 10^9$ K), and neutron densities ($> 10^{20}$ neutrons/cm^3).
– Isotopes far from stability are synthesized.

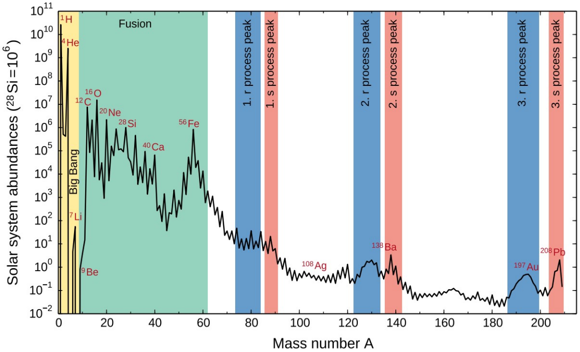

Fig. taken: A. Arcones et al., Astron Astrophys Rev **31**, 1 (2023).

T. Kajino et al., Progress in Particle and Nuclear Physics **107**, 109 (2019).

Nucleosynthesis of heavy elements: competition b/w neutron capture and β decay

The origin of most atomic nuclei with masses heavier than the iron group elements is attributed to **neutron capture** nucleosynthesis

slow neutron capture process (s-process)

neutron capture << beta decay.
– Isotopes near stability are synthesized.

rapid neutron capture process (r-process)

neutron capture >> beta decay.
– Explosive environment!
– High temperatures ($T \approx 10^9$ K), and neutron densities ($> 10^{20}$ neutrons/cm^3).
– Isotopes far from stability are synthesized.

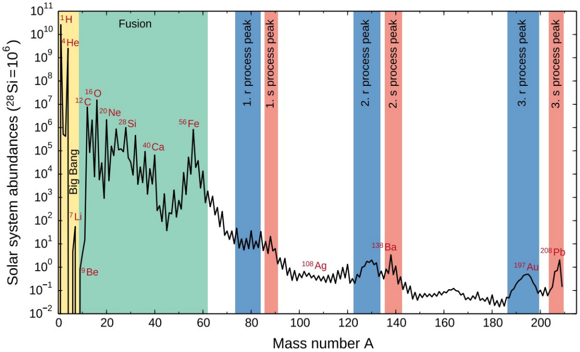

- *About half of the elements heavier than Fe are produced by* **r-process**
- *Lots of neutron-rich nuclei involved around A ~ 195, for ex. Au, Pt,...*
- *The r-process abundances strongly depend on several nuclear inputs like nuclear masses, neutron capture rates, β-decay rates, and β-delayed neutron emission process...*

Fig. taken: A. Arcones et al., Astron Astrophys Rev **31**, 1 (2023). T. Kajino et al., Progress in Particle and Nuclear Physics **107**, 109 (2019).

Importance of β-decay half-lives and β-delayed neutron emission probability in astrophysical environments

β-decay half-lives

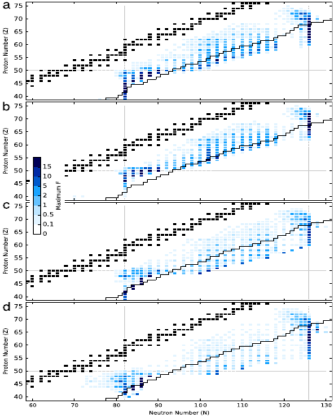

Fig. 14. Important β-decay half-lives in four astrophysical environments (a) low entropy hot wind, (b) high entropy hot wind, (c) cold wind and (d) neutron star merger with stable isotopes in black. Estimated neutron-rich accessibility limit shown by a black line for FRIB with intensity of 10^{-4} particles per second [206].

β-delayed neutron emission probabilities

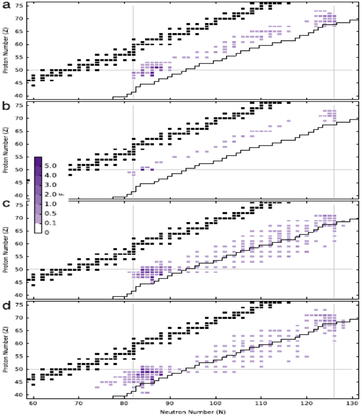

Fig. 15. Important β-delayed neutron emitters in four astrophysical environments (a) low entropy hot wind, (b) high entropy hot wind, (c) cold win and (d) neutron star merger with stable isotopes in black. Estimated neutron-rich accessibility limit shown by a black line for FRIB with intensity of 10 particles per second [206].

Credit: M.R. Mumpower, et al., Prog. Part. Nucl. Phys. **86**, 86(2016).

Importance of neutron capture rates in astrophysical environments

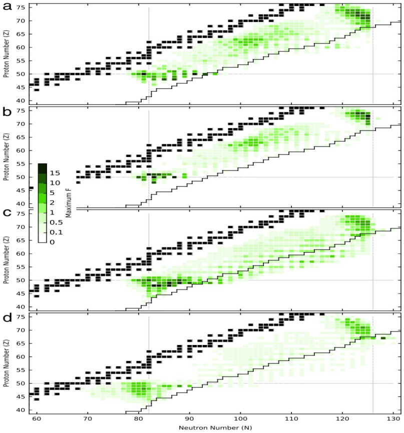

Fig. 16. Important neutron capture rates in four astrophysical environments (a) low entropy hot wind, (b) high entropy hot wind, (c) cold wind and (d) neutron star merger with stable isotopes in black. Estimated neutron-rich accessibility limit shown by a black line for FRIB with intensity of 10^{-4} particles per second [206].

Credit: M.R. Mumpower, et al., Prog. Part. Nucl. Phys. **86**, 86(2016).

Variance from the uncertain nuclear masses in abundance patterns

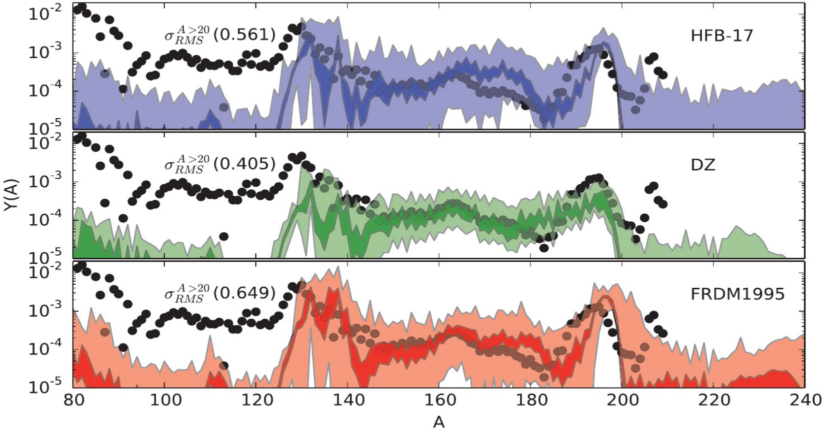

Figure 3. Variance in isotopic abundance patterns from three uncertain nuclear mass model predictions (HFB-17, DZ, and FRDM1995) compared to the solar *r*-process residuals (dots). Darker shaded band represents the same monte carlo simulation with each mass model rms error fixed at 100 keV.

Credit: M.R. Mumpower, et al., Prog. Part. Nucl. Phys. **86**, 86(2016).

Variance from the uncertain β-decay and neutron capture rates in abundance patterns

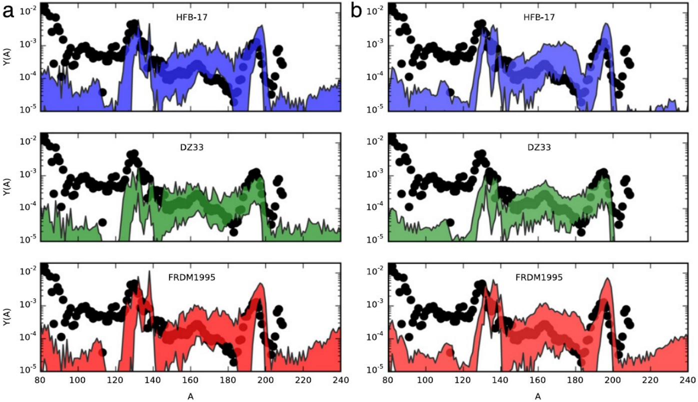

Fig. 11. Variance in isotopic abundance patterns from uncertain β-decay half-lives, panel (a) and uncertain neutron capture rates, panel (b). The same three nuclear mass model predictions (HFB-17, DZ33, and FRDM1995) and the same main ($A > 120$) r-process conditions are used as in Fig. 10.
Source: Simulation data from [200].

Credit: M.R. Mumpower, et al., Prog. Part. Nucl. Phys. **86**, 86(2016).

Experimental facilities worldwide to measure the β-decay properties

Recent experimental facilities worldwide aim to achieve precise nuclear properties:

- Nuclear masses
- Beta decay properties like β-decay half-lives and β-delayed neutron emission probabilities.

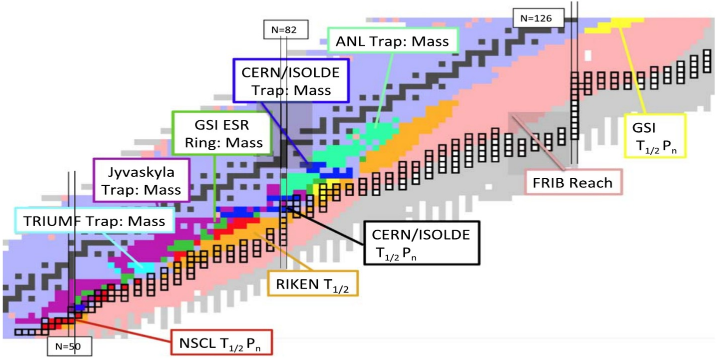

Figure 9. Recent r-process motivated experiments measuring masses or β-decay half-lives $T_{1/2}$ at various radioactive beam facilities. The colors of the legend boxes match the colors of the chart and denote a specific facility or experimental collaboration. The pink area denotes the reach of the future FRIB facility.

Credit: C J Horowitz et al, J. Phys. G: Nucl. Part. Phys. 46 083001 (2019).

Gamow-Teller transitions strength of neutron-rich N = 82 nuclei

Gamow–Teller (GT) strength distributions have a peak in the low excitation energies and this peak, dominant by $\nu 0g_{7/2} \rightarrow \pi 0g_{9/2}$ transitions is enhanced on the proton-deficient side because the Pauli-blocking effect caused by occupying the valence proton $0g_{9/2}$ orbit is weakened.

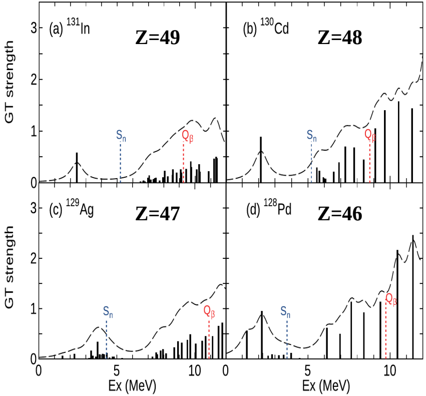

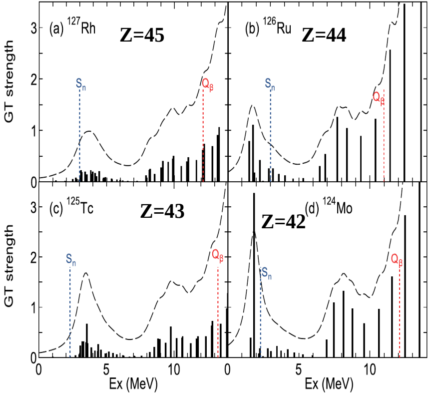

N. Shimizu, et al., Prog. Theor. Exp. Phys. **2021**, 033D01 (2021).

Gamow-Teller transitions strength of neutron-rich N = 82 nuclei

Gamow–Teller (GT) strength distributions have a peak in the low excitation energies and this peak, dominant by $\nu 0g_{7/2} \rightarrow \pi 0g_{9/2}$ transitions is enhanced on the proton-deficient side because the Pauli-blocking effect caused by occupying the valence proton $0g_{9/2}$ orbit is weakened.

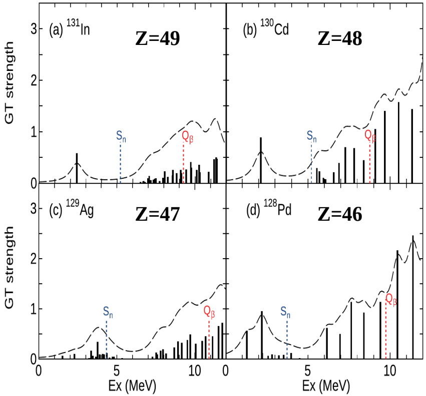

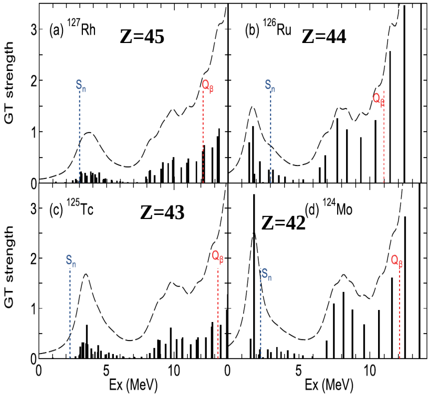

N. Shimizu, et al., Prog. Theor. Exp. Phys. **2021**, 033D01 (2021).

We also aim to investigate whether a similar situation arises for N = 126 isotones.

Aim of this study

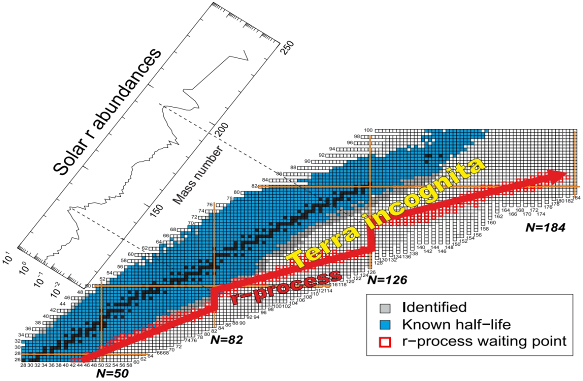

- Fig. taken: A. Evdokimov et al., “XII International Symposium on Nuclei in the Cosmos”, PoS, (2012).

Aim of this study

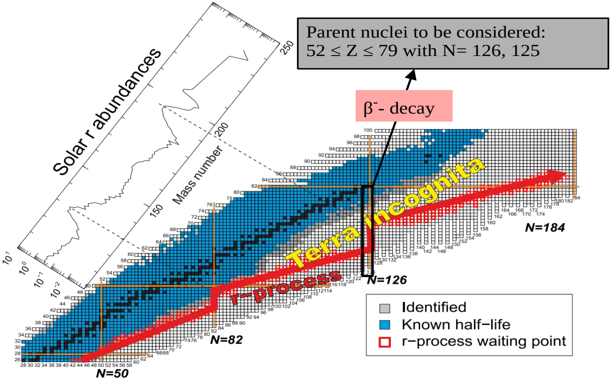

- Fig. taken: A. Evdokimov et al., "XII International Symposium on Nuclei in the Cosmos", PoS, (2012).

Aim of this study

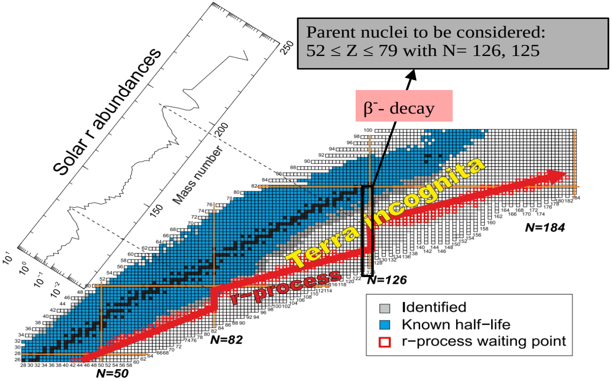

To investigate the β-decay properties like half-lives ($T_{1/2}$) and β-delayed neutron emission probabilities (P_n)

Recent developments in large-scale shell model calculations like methodology, effective interactions, and the advent of computational resources (Fugaku supercomputer) offer the opportunity to conduct demanding large-scale calculations.

To discuss the systematic study of Gamow-Teller strength distributions

▶ Fig. taken: A. Evdokimov et al., "XII International Symposium on Nuclei in the Cosmos", PoS, (2012).

Aim of this study

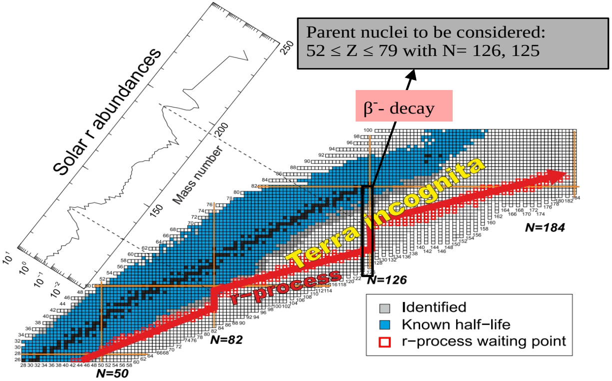

To investigate the β-decay properties like half-lives ($T_{1/2}$) and β-delayed neutron emission probabilities (P_n)

Recent developments in large-scale shell model calculations like methodology, effective interactions, and the advent of computational resources (Fugaku supercomputer) offer the opportunity to conduct demanding large-scale calculations.

To discuss the systematic study of Gamow-Teller strength distributions

- Many nuclei are particularly important to the r-process nucleosynthesis
- The predicted β-decay half-lives play crucial role in determining the r-process time scale around the 3^{rd}-peak
- Poor experimental information about the beta decay around $A \sim 195$

► Fig. taken: A. Evdokimov et al., "XII International Symposium on Nuclei in the Cosmos", PoS, (2012).

Nuclear shell-model

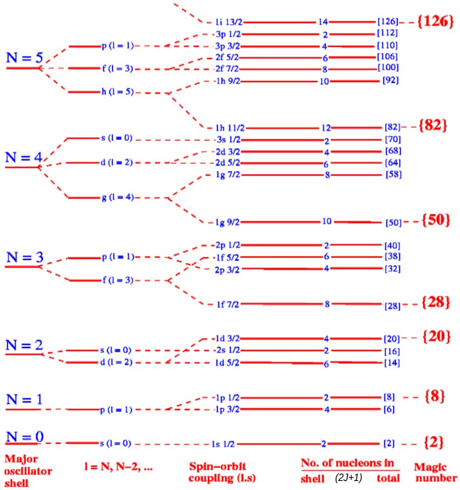

http://pms.iitk.ernet.in/wiki/index.php/The_Shell_Model

Nuclear shell-model

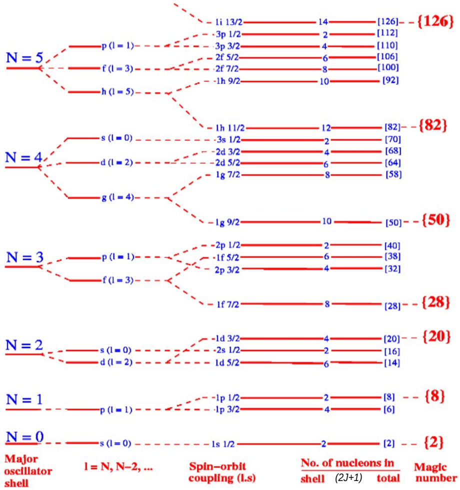

http://pms.iitk.ernet.in/wiki/index.php/The_Shell_Model

A shell model calculation needs the following ingredients:

Solve Schrondiger's Equation

$$H|\Psi\rangle = E|\Psi\rangle, \text{ where, } |\Psi\rangle = \sum_m v_m |m\rangle$$

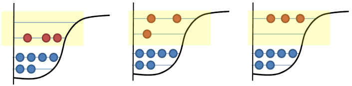

$$|\Psi\rangle = v_1|m_1\rangle + v_2|m_2\rangle + v_3|m_3\rangle + \cdots$$

- A valence space
- An effective interaction or Hamiltonian
- An efficient computer code to diagonalize the large-scale Hamiltonian matrix

Shell-model calculations: valence space

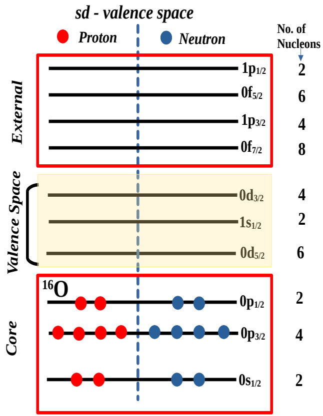

- **Define a Core**: lowest inactive region
- **A valence space**
  Valence nucleons interact through interactions
- **External space**

Effective Hamiltonian usually consists of **single-particle energies (SPEs)** and **two-body matrix elements (TBMEs)**
SPEs takes, e.g., from core+1 nucleon spectrum
TBMEs: Two-body interaction among valence nucleons

- **A standard shell-model effective Hamiltonian:**

$$H = \sum_a \varepsilon_a n_a + \sum_{a\le b, c\le d, JM} V(abcd;J) A^\dagger_{JM}(a,b) A_{JM}(c,d)$$

where $a = (n_a, l_a, j_a)$ to specify a single-particle orbit and

$$n_a = \sum_{m_a} c^\dagger_{a,m_a} c_{a,m_a} \text{ and } A^\dagger_J(a,b) = \frac{1}{\sqrt{1+\delta_{ab}}}[c^\dagger_a \otimes c^\dagger_b]^{(J)}$$

Present shell model calculations: valence space

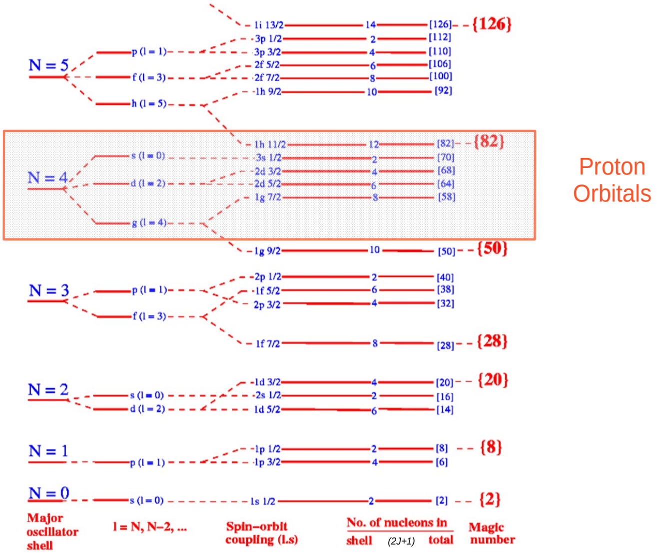

http://pms.iitk.ernet.in/wiki/index.php/The_Shell_Model

Present shell model calculations: valence space

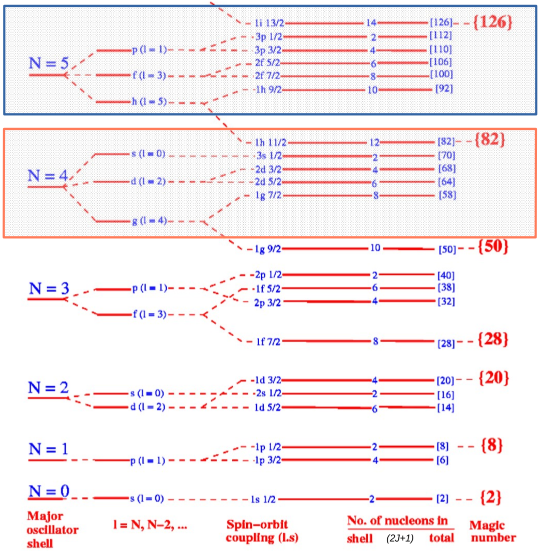

Neutron Orbitals

Proton Orbitals

http://pms.iitk.ernet.in/wiki/index.php/The_Shell_Model

Present shell model calculations: valence space

Valence space in the present calculation

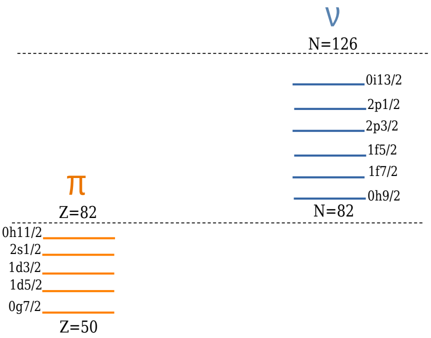

Present shell model calculations: valence space

Valence space in the present calculation

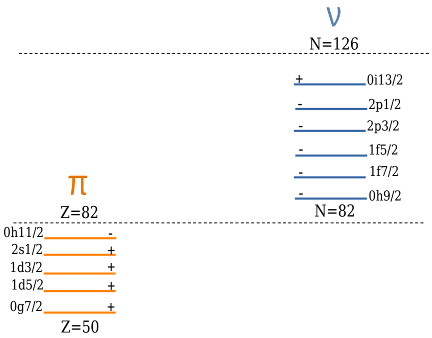

Inclusion of first-forbidden β decay

- For nuclei within this region, protons and neutrons occupy different shells with different parity

Present shell model calculations: valence space

Valence space in the present calculation

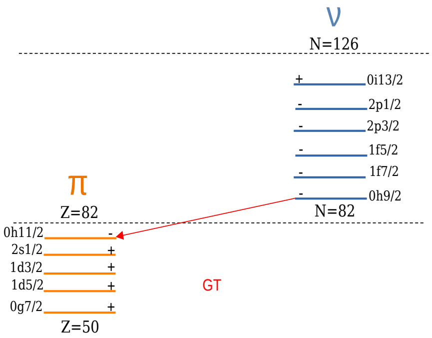

Inclusion of first-forbidden β decay

- For nuclei within this region, protons and neutrons occupy different shells with different parity
- When undergoing with β decay, only one Gamow-Teller transition $\nu 0h_{9/2} \longrightarrow \pi 0h_{11/2}$ possible with same parity ($\Delta J = 0, \pm 1$, $\Delta\pi$ = No)

Present shell model calculations: valence space

Valence space in the present calculation

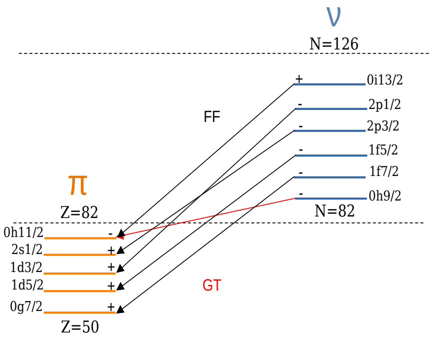

Inclusion of first-forbidden β decay

- For nuclei within this region, protons and neutrons occupy different shells with different parity
- When undergoing with β decay, only one Gamow-Teller transition $\nu 0h_{9/2} \longrightarrow \pi 0h_{11/2}$ possible with same parity ($\Delta J = 0, \pm 1$, $\Delta\pi$ = No)
- Due to parity change between two different shells of proton and neutron, becomes important to the consideration of first-forbidden transitions ($\Delta J = 0, 1, \mathbf{2}$, $\Delta\pi$ = Yes)

Present shell model calculations: valence space

Valence space in the present calculation

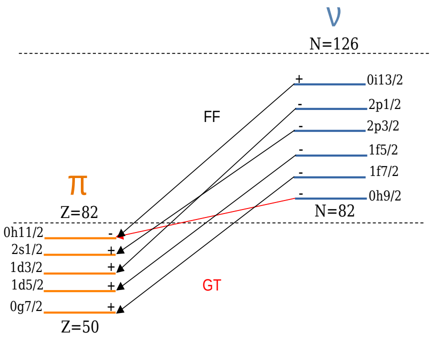

Inclusion of **first-forbidden** β decay

- For nuclei within this region, protons and neutrons occupy different shells with different parity
- When undergoing with β decay, only one Gamow-Teller transition $\nu 0h_{9/2} \longrightarrow \pi 0h_{11/2}$ possible with same parity ($\Delta J = 0, \pm 1$, $\Delta\pi$ = No)
- Due to parity change between two different shells of proton and neutron, becomes important to the consideration of first-forbidden transitions ($\Delta J = 0, 1, \mathbf{2}$, $\Delta\pi$ = Yes)

Hamiltonian

Kuo-Herling hole: KHHE Hamiltonian [1] and modified in [2]

Shell Model code:

KSHELL: MPI + OpenMP hybrid code [3]

- [1] E. K. Warburton et al., Phys. Rev. C **43**, 602 (1991).
- [2] C. Yuan et al., Phys. Rev. C **106**, 044314 (2022).
- [3] N. Shimizu et al., Computer Physics Communications **244**, 372 (2019).

Previous shell-model studies of β-decay near $N = 126$

T. Suzuki et al.

- $N = 126$ isotones with $Z = 64 - 78$

Previous

- Utilized original KHHE Hamiltonian
- Truncated model space used for $N = 126$ isotones

Present

- Utilized slightly modified KHHE Hamiltonian by C. Yuan et al.
- Performed full model space calculations for $N = 126$ isotones
- Extend $N = 126$ isotones chain to proton deficient side
- Also included $N = 125$ isotones chain in addition to $N = 126$ isotones
- Discuss the distribution of Gamow-Teller strength

Q. Zhi et al.

- $N = 126$ isotones with $Z = 66 - 73$

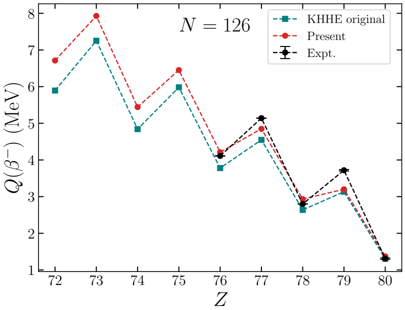

- Q. Zhi et al., Phys. Rev. C **87**, 025803 (2013).
- T. Suzuki et al., Phys. Rev. C **85**, 015802 (2012).
- T. Suzuki et al., The Astrophysical Journal **859**, 133 (2018).
- C. Yuan et al., Phys. Rev. C **106**, 044314 (2022).

Low-lying energy spectra of $N = 126, 125$ isotones

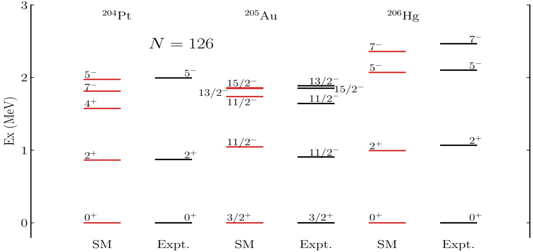

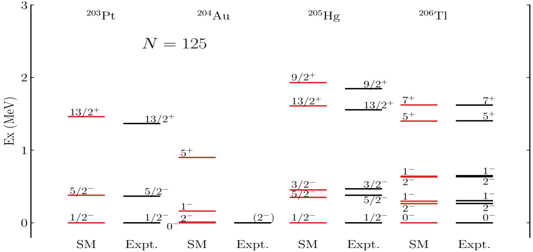

$N = 126$ nuclei

- Correctly reproduced the ground state (g.s.) spin-parities from the presently used Hamiltonian for experimentally known $N = 126$ nuclei.
- Excited states also reproduced reasonably

$N = 125$ nuclei

- Correctly reproduced the experimental ground-state spin-parities except for ^{204}Au.
- ^{204}Au: experimentally predicted g.s. (2^-), while SM predicted g.s. to be 0^-. The SM 2^- state is very close to the g. s., with an energy lying at 10 keV.

A. Kumar, N. Shimizu, Y. Utsuno, C. Yuan, and P. C. Srivastava, Phys. Rev. C 109, 064319 (2024).

$Q(\beta^-)$ values of $N = 126, 125$ isotones

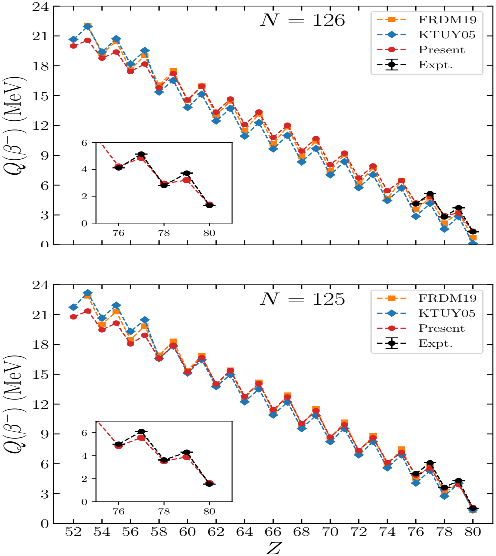

Shell model predicted $Q(\beta^-)$ values of $N = 126, 125$ isotones are compared with available experimental data and with different theoretical model calculations

$$Q(\beta^-) = E^{\text{par.}}_{\text{g.s.}} - E^{\text{dau.}}_{\text{g.s.}} + \delta m,$$

where the $\delta m = 0.782$ MeV.

- Shell model excellently reproduced the available experimental values
- Odd-even staggering is also observed similar to that observed in the FRDM19 and KTUY05 models
- Demonstrating a consistent trend with other theoretical models, such as FRDM19 and KTUY05, the predicted values are slightly smaller on the proton-deficient side.

- FRDM19: P. Möller et al., Atomic Data and Nuclear Data Tables **125**, 1 (2019).
- KTUY05: H. Koura et al., Prog. of Theo. Phys. **113**, 305 (2005).

β-decay theory

Partial half-life:

$$t_{1/2} = \frac{\kappa}{f}, \quad \text{where} \quad k = 6144 \quad \text{sec},$$

and f is the dimensionless integrated shape function, which can be expressed as

$$f = \int_1^{w_0} C(w)(w^2 - 1)^{1/2} w(w_0 - w)^2 F_0(Z, w) dw,$$

where w is the total energy of the electron and w_0 is the maximum energy of w.
The theoretical shape factor $C(w)$ is defined as

$$C(w) = \sum_{k_e, k_\nu, K} \lambda_{k_e} \Big[M_K(k_e, k_\nu)^2 + m_K(k_e, k_\nu)^2 - \frac{2\gamma_{k_e}}{k_e w_e} M_K(k_e, k_\nu) m_K(k_e, k_\nu) \Big].$$

The shape factor $C(w)$ for the Gamow-Teller transition is defined as

$$C(w) = \frac{|\mathcal{M}_{\text{GT}}|^2}{2J_i + 1}.$$

- H. Behrens, W. Bühring, *Electron Radial Wave Functions and Nuclear Beta-Decay* (Clarendon Press, Oxford, 1982).

β-decay theory

For first-forbidden β decay, the form of the shape factor $C(w)$ can be written in simple way

$$C(w) = K_0 + K_1 w + K_{-1} w^{-1} + K_2 w^2,$$

where, the coefficients $K_n (n = -1,\ 0,\ 1,\ 2)$ depend on the first-forbidden nuclear matrix elements.

Summary of GT and FF nuclear matrix elements, where $\lambda = -g_A/g_V = 1.2701(25)$, $C_1 = \sqrt{4\pi/3}Y_1$, and $C = 1/\sqrt{2J_i+1}$, $E_\gamma = Q(\beta^-) + \Delta E_C - \delta m$.

Transition	Rank	Notations	Nuclear matrix element (NME)	NME in non-relativistic approximation
GT	0	$\mathcal{M}_{GT}$	$\lambda\langle f\|\|\boldsymbol{\sigma t}_-\|\|i\rangle$	
FF	0	$\mathcal{M}_0^S$	$\lambda\sqrt{3}\langle f\|\|ir[C_1 \otimes \boldsymbol{\sigma}]^0 t_-\|\|i\rangle C$	
		$\mathcal{M}_0^T$	$\lambda\sqrt{3}\langle f\|\|\gamma_5 t_-\|\|i\rangle C$	$-\lambda\sqrt{3}\langle f\|\|(i/M_N)[\boldsymbol{\sigma} \otimes \nabla]^0 t_-\|\|i\rangle C$
	1	x	$-\langle f\|\|irC_1 t_-\|\|i\rangle C$	
		$\xi' y$	$-\langle f\|\|\boldsymbol{\alpha} t_-\|\|i\rangle C$	$E_\gamma x$
		u	$\lambda\sqrt{2}\langle f\|\|ir[C_1 \otimes \boldsymbol{\sigma}]^1 t_-\|\|i\rangle C$	
	2	z	$-2\lambda\langle f\|\|ir[C_1 \otimes \boldsymbol{\sigma}]^2 t_-\|\|i\rangle C$	

β-decay theory

To make a comparison conveniently between experiment and theory, we define the average shape factor by

$$\overline{(C(W))} = \frac{f}{f_0} = \frac{6144\ s}{f_0 t}$$

with f_0

$$f_0 = \int_1^{W_0} (W^2 - 1)^{1/2} W(W_0 - W)^2 F_0(Z, W) dW$$

To make a comparison conveniently between experiment and theory, we define the average shape factor by

$$\overline{(C(W))} = \frac{f}{f_0} = \frac{6144\ s}{f_0 t}$$

with f_0

$$f_0 = \int_1^{W_0} (W^2 - 1)^{1/2} W (W_0 - W)^2 F_0(Z, W) dW$$

Total half-life

$$\frac{1}{T_{1/2}} = \sum_f \frac{1}{t_{i\to f}}$$

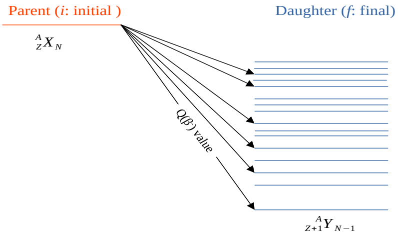

β-decay theory

To make a comparison conveniently between experiment and theory, we define the average shape factor by

$$\overline{\langle C(W) \rangle} = \frac{f}{f_0} = \frac{6144\ s}{f_0 t}$$

with f_0

$$f_0 = \int_1^{W_0} (W^2 - 1)^{1/2} W (W_0 - W)^2 F_0(Z, W) dW$$

Total half-life

$$\frac{1}{T_{1/2}} = \sum_f \frac{1}{t_{i \to f}}$$

β-delayed neutron emission probabilities:

$$P_n = \left(\sum_{E_f \geq S_n} \frac{1}{t_{i \to f}} \right) \Bigg/ \left(\sum_{\text{all } f} \frac{1}{t_{i \to f}} \right)$$

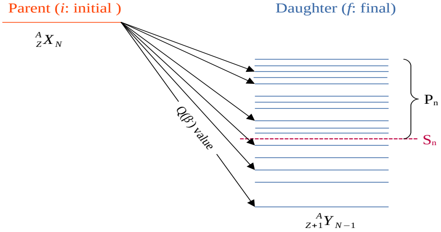

Lanczos method for strength distribution

- The β-decay half-lives are evaluated by including both the Gamow-Teller and the first-forbidden transitions.
- GT strengths are calculated using the Lanczos strength function method [1].
- The moment

$$S_k = \sum_{\nu} (E_\nu - E_i)^k |\langle \nu | \hat{O} | i \rangle|^2$$

  up to a sufficiently large k should be calculated. The Lanczos algorithm guarantees the correct moment up to $k = 2n - 1$ with n Lanczos iteration starting with $\vec{u}_1 = \hat{O}|i\rangle$.
  In this situation, one does not care about each $\langle f|\hat{O}|i\rangle$.
- In this work, the GT strengths calculated with 250 Lanczos iterations to confirm sufficiently converged results for $N = 126, 125$ isotones.

[1] R. R. Whitehead, Moment methods and lanczos methods, in Theory and Applications of Moment Methods in Many-Fermion Systems, edited by B. J. Dalton, S. M. Grimes, J. D. Vary, and S. A. Williams (Plenum, New York, 1980), p. 235.

Lanczos method for strength distribution: Example ^{48}Ca

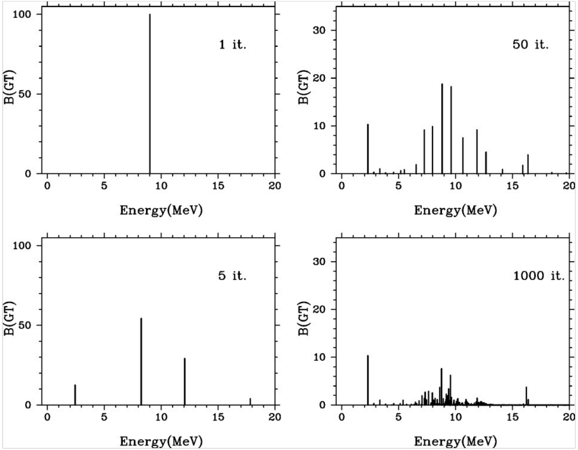

- Results from: E. Caurier et al., Rev. Mod. Phys. **77**, 427 (2005).

Lanczos method for strength distribution: Example ^{48}Ca

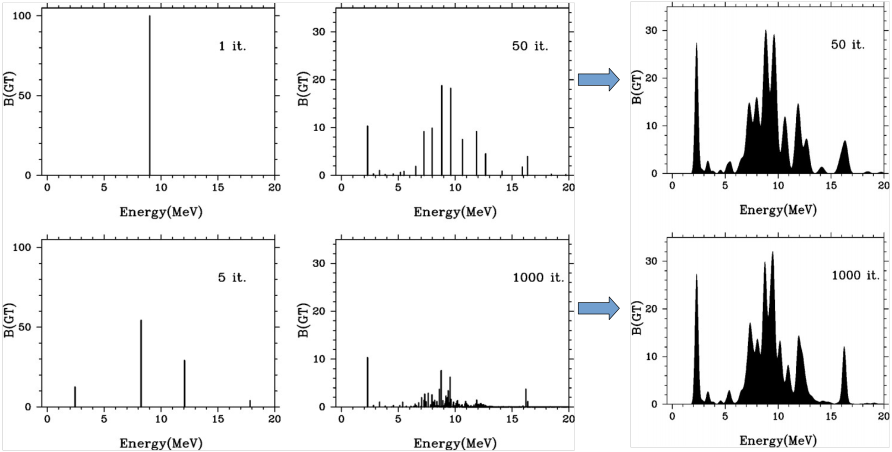

- After 50 iterations, a good distribution is achieved, despite notable variations in individual strengths between 50 and 1000 iterations.

▶ Results from: E. Caurier et al., Rev. Mod. Phys. **77**, 427 (2005).

Monopole-based truncation

- In case of first-forbidden β decay: due to the involvement of six operators, the first-forbidden strength has been obtained by diagonalization of the Hamiltonian and calculated strength for 50 eigenvalues for each state in the daughter nuclei

- Full model space diagonalized:
  $N = 126$ isotones with $Z = 52 - 79$ and
  $N = 125$ isotones with $Z = 52 - 59$ and $Z = 72 - 79$
- Due to the limitation of computational resources, monopole-based truncation is applied on $\boldsymbol{N = 125}$ isotones with $\boldsymbol{Z = 60 - 71}$

Monopole-based truncation

- In case of first-forbidden β decay: due to the involvement of six operators, the first-forbidden strength has been obtained by diagonalization of the Hamiltonian and calculated strength for 50 eigenvalues for each state in the daughter nuclei

- Full model space diagonalized:
  $N = 126$ isotones with $Z = 52 - 79$ and
  $N = 125$ isotones with $Z = 52 - 59$ and $Z = 72 - 79$
- Due to the limitation of computational resources, monopole-based truncation is applied on $\boldsymbol{N = 125}$ isotones with $\boldsymbol{Z = 60 - 71}$
- The total monopole energy of a given partition

$$E^m_{\mathcal{P}} = \sum_j \mathcal{E}^c_j N_{\mathcal{P};j} + \sum_{j \le j'} V_{m;jj'} \frac{N_{\mathcal{P};j}\left(N_{\mathcal{P};j'} - \delta_{jj'}\right)}{1 + \delta_{jj'}}$$

Monopole-based truncation

- In case of first-forbidden β decay: due to the involvement of six operators, the first-forbidden strength has been obtained by diagonalization of the Hamiltonian and calculated strength for 50 eigenvalues for each state in the daughter nuclei

- Full model space diagonalized:
  $N = 126$ isotones with $Z = 52 - 79$ and
  $N = 125$ isotones with $Z = 52 - 59$ and $Z = 72 - 79$
- Due to the limitation of computational resources, monopole-based truncation is applied on $\boldsymbol{N = 125}$ isotones with $\boldsymbol{Z = 60 - 71}$
- The total monopole energy of a given partition

$$E^m_{\mathcal{P}} = \sum_j \mathcal{E}^c_j N_{\mathcal{P};j} + \sum_{j \le j'} V_{m;jj'} \frac{N_{\mathcal{P};j}\left(N_{\mathcal{P};j'} - \delta_{jj'}\right)}{1 + \delta_{jj'}}$$

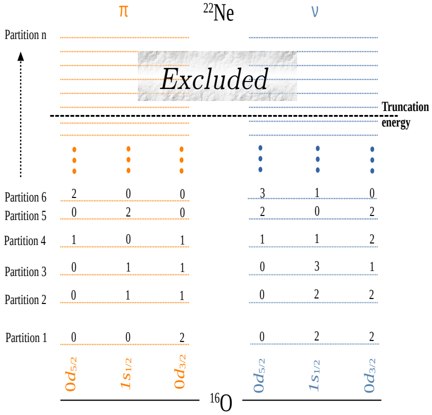

Effective operators: Gamow-Teller

To make a comparison of the shell model calculated β decay rate with the experimental one, we used effective operators in the calculations

$$\hat{O}^{\text{eff}} = q \times \hat{O}^{\text{free}}$$

where, the bare operator $\hat{O}^{\text{free}}$ is multiplied by a scaling factor (a name coined as a **quenching factor** in several earlier studies.)

To address the quenching factor in GT transitions in this study:

GT transitions for quenching factor ($q_{\text{GT}} = 0.54$)

Transition	$\lvert \mathcal{M}_{\text{GT}} \rvert$			$\log f_0 t$		
	Exp.	SM ($q = 1$)	SM ($q = 0.54$)	Exp.	SM ($q = 1$)	SM ($q = 0.54$)
$^{199}\text{Pt}(5/2^-) \rightarrow {}^{199}\text{Au}(7/2^-)$	0.114	0.297	0.160	6.45(1)	5.62	6.16
$^{200}\text{Au}^m(12^-) \rightarrow {}^{200}\text{Hg}(11^-)$	0.349	0.608	0.327	6.1(3)	5.6	6.2

Effective operators: First-forbidden

- The operators of rank 0, 1, and 2 in the first-forbidden β decay also required a quenching factor.
- To obtain quenching factors for all FF operators, we have minimized the chi-square function between theoretical and experimental average shape factors by including unique and non-unique first-forbidden transitions (**two unique and sixteen non-unique transitions**).

Experimentally know β^- first-forbidden transitions

^{205}Au$\rightarrow$ ^{205}Hg$\rightarrow$ ^{205}Tl
^{206}Hg$\rightarrow$ ^{206}Tl$\rightarrow$ ^{206}Pb (18 first-forbidden transitions)
^{207}Tl$\rightarrow$ ^{207}Pb

Quenching factors adopted in the present study

	FF				
	M_0^S	M_0^T	x	u	z
Present	0.41	1.266	0.51	0.28	0.71
Q. Zhi et al.	0.66	1.266	0.51	0.38	0.42

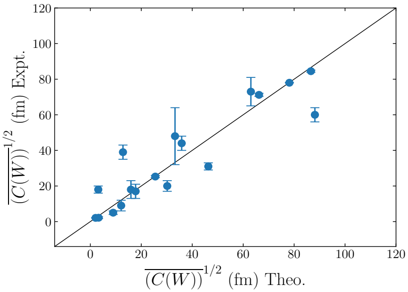

- E. K. Warburton et al., Phys. Rev. C **44**, 233 (1991).
- Q. Zhi et al., Phys. Rev. C **87**, 025803 (2013).

Converged half-lives with monopole-based truncation [Ex. ^{193}Ho, ^{196}Yb, and ^{198}Hf of $N = 126$]

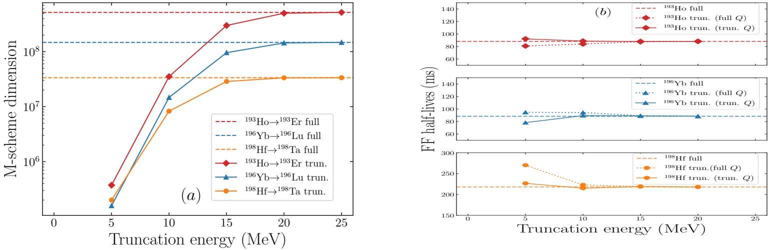

Converged half-lives with monopole-based truncation [Ex. ^{193}Ho, ^{196}Yb, and ^{198}Hf of $N = 126$]

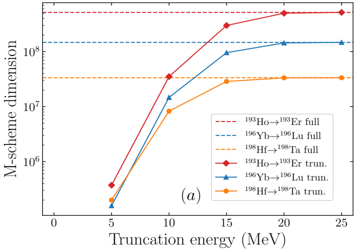

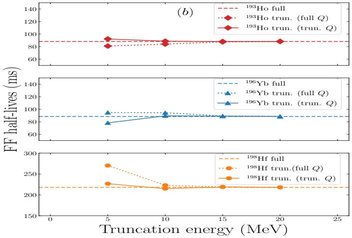

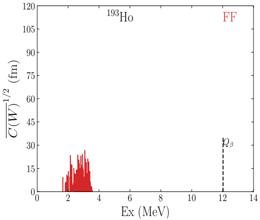

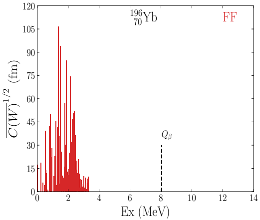

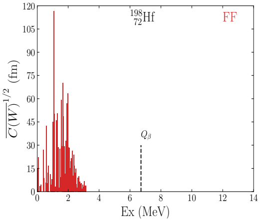

Result: Half-lives of experimentally known β decay

Shell-model predicted half-lives (sec) in comparison to the existing experimental data

	$N = 125$			$N = 126$	
	^{202}Ir	^{203}Pt	^{204}Au	^{204}Pt	^{205}Au
Present	4.7	20.6	25.4	**13.9**	23.7
Exp	15(3)	22(4)	37.2(8)	$\mathbf{16^{+6}_{-5}}$	32.5(14)
SM 2018				**38.3**	

- Exp: A. I. Morales et al., Phys. Rev. Lett. **113**, 022702 (2014).
- SM 2018: T. Suzuki et al., The Astrophysical Journal **859**, 133 (2018).

We introduce r as a measure of deviation

$$r = \log_{10}(T_{1/2}^{\text{calc}}/T_{1/2}^{\text{exp}}),$$

and its mean value and standard deviation can be written as

$$\bar{r} = \frac{1}{n}\sum_{i=1}^{n} r_i,$$

and

$$\sigma = \left[\frac{1}{n}\sum_{i=1}^{n}(r_i - \bar{r})\right]^{1/2},$$

Discrepancies of shell-model half-lives from the experimental ones

$\bar{r}$	σ	$10^{\bar{r}}$	10^{σ}	n
-0.18	0.17	0.66	1.48	5

A. Kumar, N. Shimizu, Y. Utsuno, C. Yuan, and P. C. Srivastava, Phys. Rev. C 109, 064319 (2024).

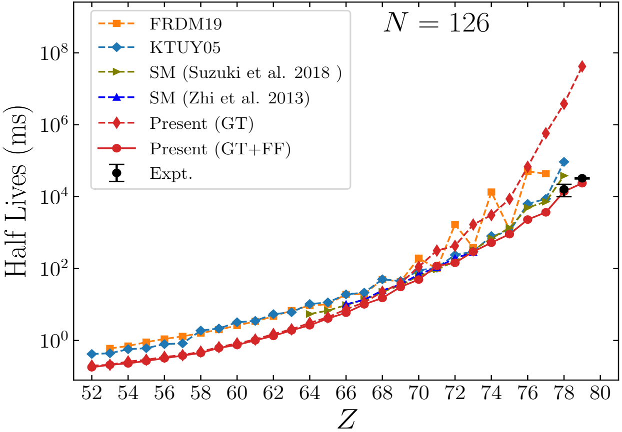

Present shell-model predicted β-decay half-lives for $N = 126$ isotones are compared with different theoretical model calculations and existing experimental data.

- FRDM19: P. Möller et al., Atomic Data and Nuclear Data Tables **125**, 1 (2019).
- KTUY05: H. Koura et al., Prog. of Theo. Phys. **113**, 305 (2005).
- SM: T. Suzuki et al., The Astrophysical Journal **859**, 133 (2018).
- SM: Q. Zhi et al., Phys. Rev. C **87**, 025803 (2013).
- Exp.: A. I. Morales et al., Phys. Rev. Lett. **113**, 022702 (2014).

A. Kumar, N. Shimizu, Y. Utsuno, C. Yuan, and P. C. Srivastava, Phys. Rev. C 109, 064319 (2024).

Result: Half-lives of $N = 126$ isotones

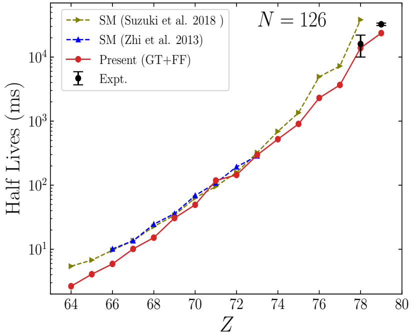

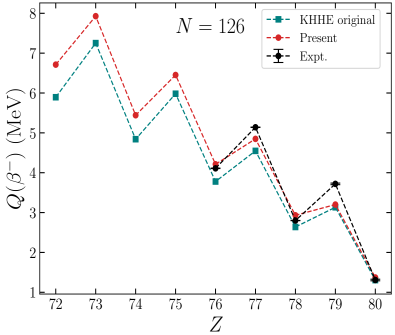

Present shell-model predicted β-decay half-lives for $N = 126$ isotones are compared with the previously shell model calculated and existing experimental data.

- SM: T. Suzuki et al., The Astrophysical Journal **859**, 133 (2018).
- SM: Q. Zhi et al., Phys. Rev. C **87**, 025803 (2013).
- Exp.: A. I. Morales et al., Phys. Rev. Lett. **113**, 022702 (2014).

A. Kumar, N. Shimizu, Y. Utsuno, C. Yuan, and P. C. Srivastava, Phys. Rev. C 109, 064319 (2024).

Result: Half-lives of $N = 125$ isotones

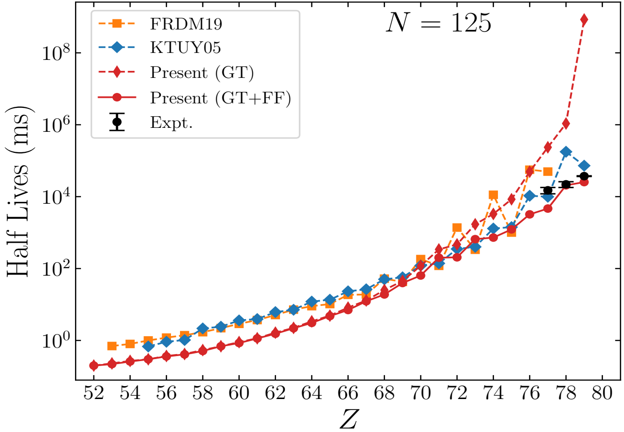

Present shell-model predicted β-decay half-lives for $N = 125$ isotones are compared with different theoretical model calculations and existing experimental data.

- FRDM19: P. Möller et al., Atomic Data and Nuclear Data Tables **125**, 1 (2019).
- KTUY05: H. Koura et al., Prog. of Theo. Phys. **113**, 305 (2005).
- Exp.: A. I. Morales et al., Phys. Rev. Lett. **113**, 022702 (2014).

A. Kumar, N. Shimizu, Y. Utsuno, C. Yuan, and P. C. Srivastava, Phys. Rev. C 109, 064319 (2024).

Result: Contribution of GT and FF transitions in Half-lives

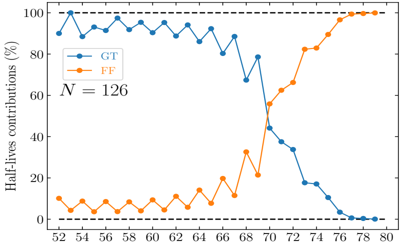

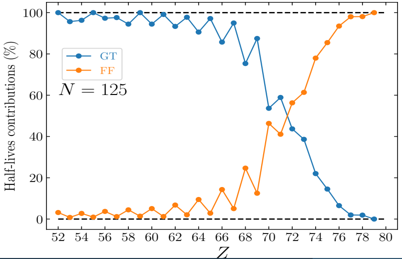

- The effect of first-forbidden transitions in the total half-lives of $N = 126$ **(top)** and $N = 125$ **(bottom)** isotones

A. Kumar, N. Shimizu, Y. Utsuno, C. Yuan, and P. C. Srivastava, Phys. Rev. C 109, 064319 (2024).

Result: Contribution of GT and FF transitions in Half-lives

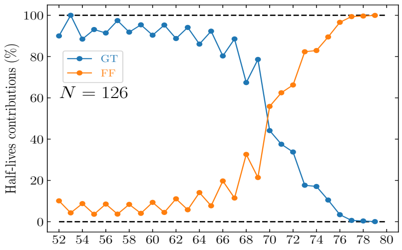

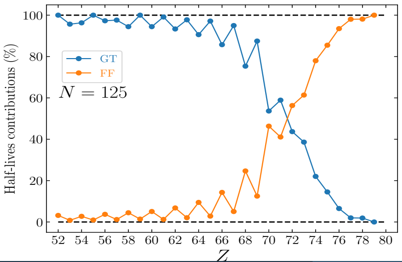

- The effect of first-forbidden transitions in the total half-lives of $N = 126$ **(top)** and $N = 125$ **(bottom)** isotones
- GT transition dominated by the $\nu 0h_{9/2} \rightarrow \pi 0h_{11/2}$

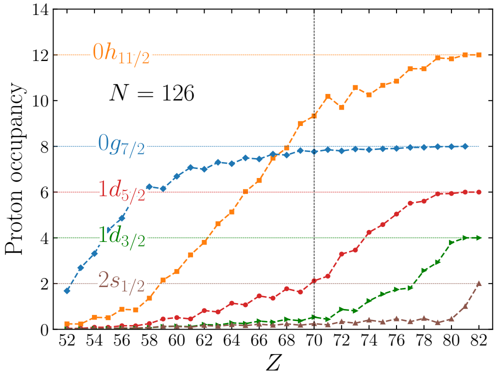

A. Kumar, N. Shimizu, Y. Utsuno, C. Yuan, and P. C. Srivastava, Phys. Rev. C 109, 064319 (2024).

Result: Gamow-Teller strength distributions of $N = 126$ isotones

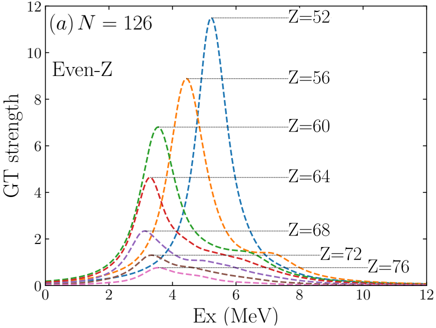

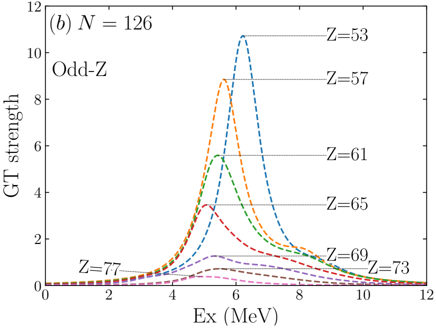

- The GT strength peaks are observed at low excitation energies between 3-6 MeV and 5-7 MeV for even-Z and odd-Z of parent nuclei, respectively.
- This peak, dominated by the $\nu 0h_{9/2} \rightarrow \pi 0h_{11/2}$ transition, is enhanced on the proton deficient side because the Pauli-blocking effect caused by the occupying the valence proton $0h_{11/2}$ orbit is weakened.

Result: Total GT strength distributions as a function of $\pi 0h_{11/2}$ orbit

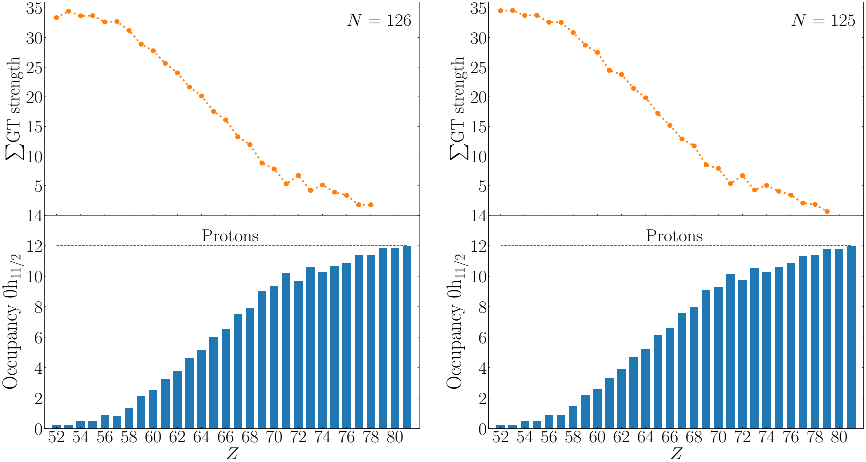

- As the proton number increases, the proton $0h_{11/2}$ orbit becomes occupied, and simultaneously, the sum of GT strength decreases due to the **Pauli blocking effect**, reaching almost zero near $Z = 82$.

Result: β-delayed neutron emission probabilities $P_n(\%)$

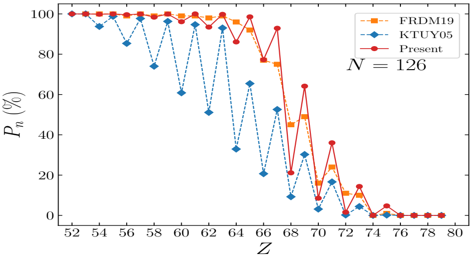

- No experimental information available about the β-delayed neutron emission probabilities $P_n(\%)$ in this region

- FRDM19: P. Möller et al., Atomic Data and Nuclear Data Tables **125**, 1 (2019).
- KTUY05: H. Koura et al., Prog. of Theo. Phys. **113**, 305 (2005).

A. Kumar, N. Shimizu, Y. Utsuno, C. Yuan, and P. C. Srivastava, Phys. Rev. C 109, 064319 (2024).

Result: β-delayed neutron emission probabilities $P_n(\%)$

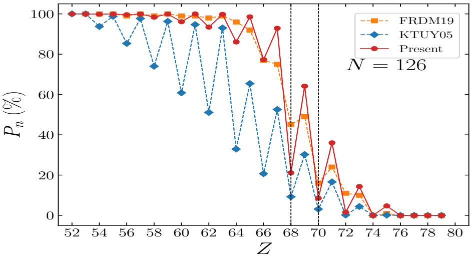

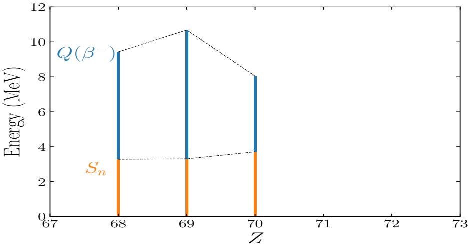

- No experimental information available about the β-delayed neutron emission probabilities $P_n(\%)$ in this region

---

- Even-odd staggering due to phase space

- FRDM19: P. Möller et al., Atomic Data and Nuclear Data Tables **125**, 1 (2019).
- KTUY05: H. Koura et al., Prog. of Theo. Phys. **113**, 305 (2005).

A. Kumar, N. Shimizu, Y. Utsuno, C. Yuan, and P. C. Srivastava, Phys. Rev. C 109, 064319 (2024).

Result: β-delayed neutron emission probabilities $P_n(\%)$

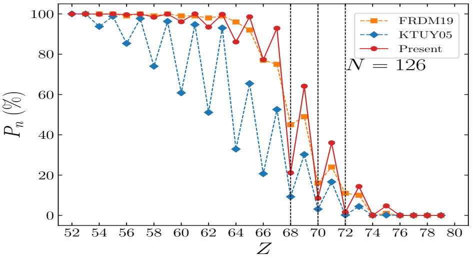

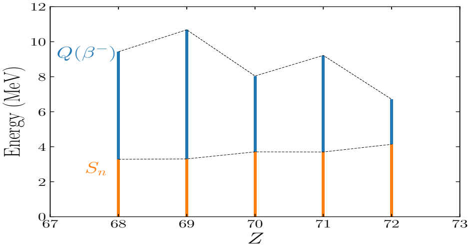

- No experimental information available about the β-delayed neutron emission probabilities $P_n(\%)$ in this region

---

- Even-odd staggering due to phase space

- FRDM19: P. Möller et al., Atomic Data and Nuclear Data Tables **125**, 1 (2019).
- KTUY05: H. Koura et al., Prog. of Theo. Phys. **113**, 305 (2005).

A. Kumar, N. Shimizu, Y. Utsuno, C. Yuan, and P. C. Srivastava, Phys. Rev. C 109, 064319 (2024).

Summary and Conclusion:

Summary:

- We have made large-scale shell model calculations to investigate the β decay properties of $N = 126$ and $N = 125$ isotones ($52 \leq Z \leq 79$) with the inclusion of first-forbidden transitions.

- Good agreement between shell model predicted and available experimental data.

- The contribution from first-forbidden transitions are important, especially for nuclei around $N = 126$ region.

- The present study of β-decay properties of waiting point nuclei around $A \approx 195$ will be add more information in the third r-process abundance peak distributions.

Future:

- **Further, we will analyze the impact of the present calculated β-decay half-lives and β-delayed neutron emission probability on the r-process abundance distribution.**